

Proposal for a Bell Test with Entangled Atoms of Different Mass

X. T. Yan, S. Kannan, Y. S. Athreya, A. G. Truscott, and S. S. Hodgman

Research School of Physics, Australian National University, Canberra 2601, Australia
2025 Jan 21

We propose a Bell test experiment using momentum-entangled atom pairs of different masses, specifically metastable helium isotopes $^3\text{He}^*$ and $^4\text{He}^*$, though the method extends to other atom species. Entanglement is generated via collisions, after which the quantum states are manipulated using two independent atom interferometers, enabling precise phase control over each species. Numerical simulations predict a significant violation of Bell's inequality under realistic conditions. This proposal opens a new paradigm to study the intersection of quantum mechanics and gravity.

1 Introduction

One of the most intriguing features of quantum mechanics is the phenomenon of entanglement, where two or more entangled particles exhibit seemingly non-local correlations that defy classical intuition, challenging the concept of local realism. This has led to suggestions that quantum mechanics might be incomplete [1] and that hidden variables could account for the observed correlations to preserve local realism. To address this, John Bell formulated a way to experimentally distinguish between the predictions of quantum mechanics and those of local hidden variable theories (LHVTs) through measuring a violation of a so-called Bell inequality [2], later made more experimentally accessible by Clauser-Horne-Shimony-Holt (CHSH) [3]. Historically, Bell tests have predominantly investigated various photonic degrees of freedom [4, 5, 6, 7, 8, 9, 10]. While lesser in number, Bell tests using atoms and electrons have so far primarily explored the internal degrees of freedom such as spin [11, 12, 13, 14]. While these experiments have provided strong evidence against local hidden variable theories, there remains a lack of experimental evidence for Bell tests involving the external degrees of freedom (momentum) of massive particles.

Attempts at atomic momentum entanglement for Bell tests have faced significant experimental challenges [15]. Dussarrat *et al.* [16] experimentally interfered different modes of two particles and ruled out the possibility of a mixed state. Fadel *et al.* [17]

S. S. Hodgman: sean.hodgman@anu.edu.au

and Lange *et al.* [18] showed spatial entanglement in cold atom experiments. Shin *et al.* [13] demonstrated Bell correlations between separated atomic pairs, using momentum as their particle label and atomic spin states to show entanglement in spin. Other attempts to produce entanglement in atomic momentum [19, 20, 16, 21], while successfully showing forms of non-classical correlations, possessed insufficient coherence to perform a full Bell test. Our recent attempt [22] used mixing between different momentum states in two separate s -wave scattering halos of metastable helium ($^4\text{He}^*$) atoms to perform a Bell test [23], although with insufficient visibility to exclude LHVTs.

In this paper, we propose an experiment to test a Bell inequality using momentum-entangled atoms, specifically two isotopes of $^4\text{He}^*$, although the scheme would also work with other species. By inducing controlled collisions between these isotopes and utilising species-specific momentum-transfer pulses for independent control, we generate and manipulate entangled pairs suitable for a Bell test. We present theoretical modeling of the entangled state generation, followed by numerical simulations that demonstrate a violation of the Clauser-Horne-Shimony-Holt (CHSH) inequality under realistic experimental conditions.

2 Proposed Experimental Setup

Entangled state generation. We start by creating an entangled state through collisions between two atomic species, in our case, the fermionic and bosonic isotopes of metastable helium [24], denoted as \mathcal{A} ($^3\text{He}^*$) and \mathcal{B} ($^4\text{He}^*$) respectively, initially in a harmonic trap. After switching off the trap, we transfer the \mathcal{B} atoms into a coherent superposition of momentum states moving upwards ($+\mathbf{p}_k$) and downwards ($-\mathbf{p}_k$), while the \mathcal{A} atoms remain at rest (see Fig. 1.(a)). The transfer is achieved via a two-photon Bragg transition, transferring momentum $\pm\mathbf{p}_k$ to the atoms, where $\mathbf{p}_k = \hbar(\mathbf{k}_2^{\mathcal{B}} - \mathbf{k}_1^{\mathcal{B}})$ and $\mathbf{k}_{1,2}^{\mathcal{B}}$ are the two beam wavevectors associated with the laser beams that induce the two-photon transition of \mathcal{B} [25, 22]. This momentum transfer leads to s -wave collisions between individual $^3\text{He}^*$ and $^4\text{He}^*$ atoms, with collisions occurring between pairs with momenta either $+\mathbf{p}_k$ and 0 or $-\mathbf{p}_k$ and 0. Each of these collisions will

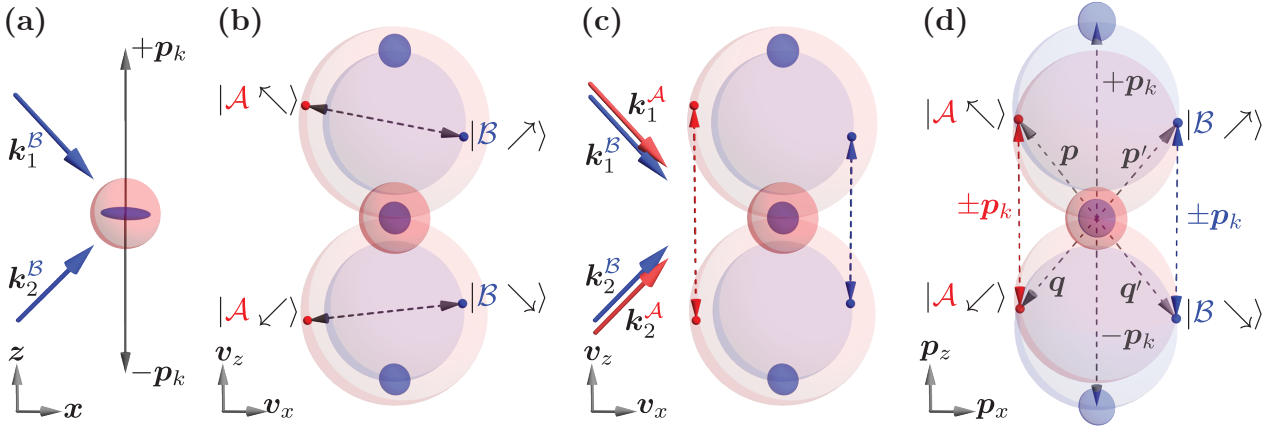


Fig. 1: Schematic of our proposed Bell test. **(a)** Initially, we prepare a ${}^3\text{He}^*$ DFG (\mathcal{A} - shown in red) and a ${}^4\text{He}^*$ BEC (\mathcal{B} - shown in blue) overlapping in a trapping potential (not shown). The potential is switched off, and we apply laser beams with wavevectors $k_1^{\mathcal{B}}$ and $k_2^{\mathcal{B}}$ to induce a Bragg process, transferring ${}^4\text{He}^*$ (\mathcal{B}) into an equal superposition of two momentum states $\pm\hbar(\mathbf{k}_2^{\mathcal{B}} - \mathbf{k}_1^{\mathcal{B}}) =: \pm\mathbf{p}_k$. These momentum components travel through the at-rest \mathcal{A} atoms and cause individual pairs of \mathcal{A} and \mathcal{B} atoms to undergo s -wave collisions. **(b)** These collisions form two scattering halos in velocity space (faded red and blue spheres) for each of the two initial momenta $\pm\mathbf{p}_k$. By energy-momentum conservation, each \mathcal{A} atom at a particular point on the \mathcal{A} scattering halo will have a corresponding \mathcal{B} atom on the diametrically opposite point on the corresponding \mathcal{B} halo. Two example pairs $|\mathcal{A} \nearrow\rangle |\mathcal{B} \nearrow\rangle$ from the $+\mathbf{p}_k$ halos and $|\mathcal{A} \searrow\rangle |\mathcal{B} \searrow\rangle$ from the $-\mathbf{p}_k$ halos are indicated. **(c)** The addition of a second pair of Bragg beams resonant with \mathcal{A} atoms that overlap with the \mathcal{B} beams $\hat{\mathbf{k}}_{1,2}^{\mathcal{A}} = \hat{\mathbf{k}}_{1,2}^{\mathcal{B}}$, allows us to couple the upper and lower halo atoms of the same species $|\mathcal{A} \nearrow\rangle \leftrightarrow |\mathcal{A} \searrow\rangle$ and $|\mathcal{B} \nearrow\rangle \leftrightarrow |\mathcal{B} \searrow\rangle$ independently, which enables the mixing between states for a Bell test. **(d)** Corresponding momentum space distribution of the collision generated states $|\psi\rangle_{\text{upper}}$ and $|\psi\rangle_{\text{lower}}$ as described in Eqn (4). See main text for details.

produce two scattering halos [26, 27, 28], such that for every ${}^3\text{He}^*$ atom detected in one halo, a ${}^4\text{He}^*$ atom will be found in the diametrically opposite point in the other halo of the pair (see Fig. 1.(b)). Notably, ${}^4\text{He}^*$ - ${}^4\text{He}^*$ scatterings as absent in this setup, as there are no ${}^4\text{He}^*$ atoms left in the zero momentum states.

The effective Hamiltonian \hat{H}_{FWM} describing the four-wave mixing (FWM) process responsible for the pair production comes from extending the previous theoretical framework of FWM for pure bosonic atoms [29, 30, 31, 22] and pure fermions [32], to a Bose-Fermi (${}^4\text{He}^*$ - ${}^3\text{He}^*$) mixture system. This gives:

$$\hat{H}_{\text{FWM}} = \sum_{\mathbf{p}} \hbar\zeta (\hat{b}_{\mathbf{p}}^\dagger \hat{f}_{\mathbf{p}'}^\dagger + \hat{b}_{\mathbf{p}} \hat{f}_{\mathbf{p}'}), \quad (1)$$

where $\hat{b}_{\mathbf{p}}^\dagger$ and $\hat{f}_{\mathbf{p}'}^\dagger$ are the bosonic and fermionic creation operators for the ${}^4\text{He}^*$ and ${}^3\text{He}^*$ atoms, respectively. ζ is the coupling strength of this interaction depending on the scattering length and density. The summation over momenta \mathbf{p} accounts for the ${}^4\text{He}^*$ atoms with momentum \mathbf{p} and ${}^3\text{He}^*$ atoms with momentum \mathbf{p}' that satisfy both momentum conservation $\mathbf{p} + \mathbf{p}' = +\mathbf{p}_k$ and energy conservation. Consequently, only specific outgoing momenta \mathbf{p} and \mathbf{p}' are allowed, resulting in the formation of spherical halos in velocity and momentum space as depicted in Fig. 1.(b) and Fig. 1.(d) respectively.

An initial vacuum state $|\text{vac}\rangle$ then evolves under

the unitary evolution operator to obtain $U(t)$ as

$$\begin{aligned} \hat{U}(t) |\text{vac}\rangle &= e^{-\frac{i}{\hbar} \hat{H}t} \\ &= |\text{vac}\rangle + i\zeta t \sum_{\mathbf{p}} \hat{b}_{\mathbf{p}}^\dagger \hat{f}_{\mathbf{p}'}^\dagger |\text{vac}\rangle + \dots \end{aligned} \quad (2)$$

where higher-order terms involving the creation of multiple pairs into the same $(\mathbf{p}, \mathbf{p}')$ are not possible due to the antisymmetry of fermions (Pauli exclusion) [32], leaving only the vacuum state or one pair of excitations in the same \mathbf{p} . The state after FWM can therefore be approximated as a two-mode squeezed vacuum state for each scattering direction around the halo.

For the upper halo (momentum $+\mathbf{p}_k$), the state is

$$|\psi\rangle_{\text{upper}} \simeq \sum_{\mathbf{p}} \left(|0\rangle_{\mathbf{p}}^{\mathcal{A}} |0\rangle_{\mathbf{p}'}^{\mathcal{B}} + \tilde{\zeta} |1\rangle_{\mathbf{p}}^{\mathcal{A}} |1\rangle_{\mathbf{p}'}^{\mathcal{B}} \right), \quad (4)$$

where $\tilde{\zeta} = i\zeta t$ and $|n\rangle_{\mathbf{p}, \mathbf{p}'}^{\mathcal{A}, \mathcal{B}}$ denote an n -atom Fock state of ${}^3\text{He}^*$ and ${}^4\text{He}^*$ atoms with momenta \mathbf{p} and \mathbf{p}' , respectively. The lower halo will be the same but replacing \mathbf{p}, \mathbf{p}' with \mathbf{q}, \mathbf{q}' , with $\mathbf{q} + \mathbf{q}' = -\mathbf{p}_k$.

The total state is then the tensor product of the upper and lower halo states:

$$\begin{aligned} |\Psi\rangle &= |\psi\rangle_{\text{upper}} |\psi\rangle_{\text{lower}} = \sum_{\mathbf{p}} \sum_{\mathbf{q}} |0\rangle_{\mathbf{p}}^{\mathcal{A}} |0\rangle_{\mathbf{p}'}^{\mathcal{B}} |0\rangle_{\mathbf{q}}^{\mathcal{A}} |0\rangle_{\mathbf{q}'}^{\mathcal{B}} \\ &\quad + \tilde{\zeta} |1\rangle_{\mathbf{p}}^{\mathcal{A}} |1\rangle_{\mathbf{p}'}^{\mathcal{B}} |0\rangle_{\mathbf{q}}^{\mathcal{A}} |0\rangle_{\mathbf{q}'}^{\mathcal{B}} + \tilde{\zeta} |0\rangle_{\mathbf{p}}^{\mathcal{A}} |0\rangle_{\mathbf{p}'}^{\mathcal{B}} |1\rangle_{\mathbf{q}}^{\mathcal{A}} |1\rangle_{\mathbf{q}'}^{\mathcal{B}} \\ &\quad + \tilde{\zeta}^2 |1\rangle_{\mathbf{p}}^{\mathcal{A}} |1\rangle_{\mathbf{p}'}^{\mathcal{B}} |1\rangle_{\mathbf{q}}^{\mathcal{A}} |1\rangle_{\mathbf{q}'}^{\mathcal{B}}. \end{aligned} \quad (5)$$

$$+ \tilde{\zeta}^2 |1\rangle_{\mathbf{p}}^{\mathcal{A}} |1\rangle_{\mathbf{p}'}^{\mathcal{B}} |1\rangle_{\mathbf{q}}^{\mathcal{A}} |1\rangle_{\mathbf{q}'}^{\mathcal{B}}. \quad (6)$$

These terms represent the vacuum state, the single pair production in the upper and lower halo, and the two-pair production, respectively.

Since $\zeta \ll 1$ [22, 23], the two-pair term (6) is negligible compared to the single-pair terms (5). We can also post-select events where only one pair of atoms is produced and focus on the superposition of the second and third terms. As shown in Fig. 1.(d), we select \mathbf{p} , \mathbf{q} momenta satisfying $\mathbf{p} - \mathbf{q} = \mathbf{p}_k$. Notably, this geometry guarantees that the corresponding momenta \mathbf{p}' and \mathbf{q}' also satisfy $\mathbf{p}' - \mathbf{q}' = \mathbf{p}_k$, thus achieving a consistent vertical momentum transfer across selected pairs, realising a momentum mirror and beam-splitter. This is required due to the different momenta of the $^3\text{He}^*$ and $^4\text{He}^*$ components of each of the two halos. For notational simplicity, we define:

$$\begin{aligned} |\mathcal{A}, \nearrow\rangle &\equiv |1\rangle_{\mathbf{p}}^{\mathcal{A}} |0\rangle_{\mathbf{q}}^{\mathcal{A}}, & |\mathcal{A}, \searrow\rangle &\equiv |0\rangle_{\mathbf{p}}^{\mathcal{A}} |1\rangle_{\mathbf{q}}^{\mathcal{A}}, \\ |\mathcal{B}, \nearrow\rangle &\equiv |1\rangle_{\mathbf{p}'}^{\mathcal{B}} |0\rangle_{\mathbf{q}'}^{\mathcal{B}}, & |\mathcal{B}, \searrow\rangle &\equiv |0\rangle_{\mathbf{p}'}^{\mathcal{B}} |1\rangle_{\mathbf{q}'}^{\mathcal{B}}. \end{aligned} \quad (7)$$

Thus, the entangled state of interest is,

$$|\psi\rangle = |\mathcal{A} \nearrow\rangle |\mathcal{B} \nearrow\rangle + |\mathcal{A} \searrow\rangle |\mathcal{B} \searrow\rangle, \quad (8)$$

where the arrows denote their momentum directions.

Although the collision excites many pairs in various directions, we can concentrate only on pairs along a specific direction for clarity. This is possible as the Pauli exclusion principle ensures that the pair creation (3) can only generate a maximum of one pair in any particular momentum state. The cylindrical symmetry of the halos will allow this analysis to then be extended to multiple independent sets of pairs in different directions, increasing the experimental data acquisition rate.

Independent Bragg Pulses. Coupling between upper and lower halo states is achieved with separate Bragg laser pulses, tuned in phase and amplitude to function as atomic momentum mirrors and beam-splitters. These utilise the distinct transition frequencies of the $2^3S_1 \rightarrow 2^3P_0$ states of $^3\text{He}^*$ (276.7322 THz) and $^4\text{He}^*$ (276.6986 THz) [24, 33]. The laser frequencies are adjusted to match the atomic resonances of one isotope while being sufficiently detuned from the other [24, 34], allowing independent coupling of each species. The Bragg pulse induces momentum transfer through an effective unitary transformation given by [22]:

$$\begin{aligned} |\mathcal{X}, \uparrow\rangle &\xrightarrow{\hat{U}_{\varphi, \theta}^{\mathcal{X}}} \cos \frac{\theta_{\mathcal{X}}}{2} |\mathcal{X}, \uparrow\rangle - ie^{i\varphi_{\mathcal{X}}} \sin \frac{\theta_{\mathcal{X}}}{2} |\mathcal{X}, \downarrow\rangle \\ |\mathcal{X}, \downarrow\rangle &\xrightarrow{\hat{U}_{\varphi, \theta}^{\mathcal{X}}} -ie^{-i\varphi_{\mathcal{X}}} \sin \frac{\theta_{\mathcal{X}}}{2} |\mathcal{X}, \uparrow\rangle + \cos \frac{\theta_{\mathcal{X}}}{2} |\mathcal{X}, \downarrow\rangle, \end{aligned} \quad (9)$$

where $\mathcal{X} \in \{\mathcal{A}, \mathcal{B}\}$ and \uparrow represents \nearrow for \mathcal{A} or \nearrow for \mathcal{B} and \downarrow represents \searrow for \mathcal{A} or \searrow for \mathcal{B} . $\theta_{\mathcal{X}} = \Omega_{\mathcal{X}} t_{\mathcal{X}}$, with $\Omega_{\mathcal{X}}$ the Rabi frequency and $t_{\mathcal{X}}$ the laser pulse

duration, so that $\theta_{\mathcal{X}} = \pi$ represents a mirror and $\theta_{\mathcal{X}} = \pi/2$ is a beam splitter. $\varphi_{\mathcal{X}}$ is the relative laser phase between the k_1, k_2 beams and sets the phases for the Bell test.

The Bell Test. A key requirement for performing a Bell test using momentum-entangled atoms is the ability to mix different momentum states coherently [23]. However, atoms in distinct momentum states propagate along separate trajectories and become spatially separated over time. This spatial separation introduces an additional degree of freedom, position, making the states distinguishable. To allow effective mixing and interference of the momentum states, we need to bring them back into spatial overlap. We achieve this by applying mirror pulses ($\hat{U}_{\varphi_{\mathcal{A}}, \pi}^{\mathcal{A}} \hat{U}_{\varphi_{\mathcal{B}}, \pi}^{\mathcal{B}}$) to both species at t_1 after the entangled state is created, reversing the momentum of each atom. This causes the momentum states to converge and overlap in space at a later time t_2 . At the moment of overlap, we perform the beam-splitter operation ($\hat{U}_{\varphi_{\mathcal{A}}, \pi/2}^{\mathcal{A}} \hat{U}_{\varphi_{\mathcal{B}}, \pi/2}^{\mathcal{B}}$) at t_2 with variable phases ($\varphi_{\mathcal{A}}$ and $\varphi_{\mathcal{B}}$) to perform the Bell test.

After applying the mirror (π) pulse and a 50:50 beam-splitter ($\pi/2$) pulse with phases $\varphi_{\mathcal{A}}$ and $\varphi_{\mathcal{B}}$ to each species, the state evolves to

$$|\psi_{t_2}\rangle = \hat{U}_{\varphi_{\mathcal{A}}, \pi/2}^{\mathcal{A}} \hat{U}_{\varphi_{\mathcal{B}}, \pi/2}^{\mathcal{B}} |\psi_{t_1}\rangle \quad (10)$$

$$= \frac{1}{2\sqrt{2}} (-1 + e^{-i\varphi_{\mathcal{A}} - i\varphi_{\mathcal{B}}}) |\mathcal{A} \nearrow\rangle |\mathcal{B} \nearrow\rangle \quad (11)$$

$$+ \frac{i}{2\sqrt{2}} (e^{-i\varphi_{\mathcal{A}}} + e^{i\varphi_{\mathcal{B}}}) |\mathcal{A} \nearrow\rangle |\mathcal{B} \searrow\rangle \quad (12)$$

$$+ \frac{i}{2\sqrt{2}} (e^{i\varphi_{\mathcal{A}}} + e^{-i\varphi_{\mathcal{B}}}) |\mathcal{A} \searrow\rangle |\mathcal{B} \nearrow\rangle \quad (13)$$

$$+ \frac{1}{2\sqrt{2}} (-1 + e^{i\varphi_{\mathcal{A}} + i\varphi_{\mathcal{B}}}) |\mathcal{A} \searrow\rangle |\mathcal{B} \searrow\rangle. \quad (14)$$

Thus four joint momentum states are key to the Bell inequality. The probabilities for detecting atoms in each of the states \circ, \bullet are

$$P_{\circ, \bullet} = |\langle \circ, \bullet | \psi_{t_3} \rangle|^2 = \frac{1 \pm \cos(\varphi_{\mathcal{A}} + \varphi_{\mathcal{B}})}{4}, \quad (15)$$

with the $-$ case for $\langle \circ, \bullet | = \langle \mathcal{A} \nearrow | \langle \mathcal{B} \nearrow |, \langle \mathcal{A} \searrow | \langle \mathcal{B} \searrow |$ and the $+$ case for $\langle \circ, \bullet | = \langle \mathcal{A} \nearrow | \langle \mathcal{B} \searrow |, \langle \mathcal{A} \searrow | \langle \mathcal{B} \nearrow |$. This probability $P_{\circ, \bullet}$ then corresponds to the experimentally measurable [22, 13] second-order correlation function defined as [27]

$$g_{\circ, \bullet}^{(2)} = \frac{\int d\phi \langle : \hat{n}_{\circ\phi}^{\mathcal{A}} \hat{n}_{\bullet\phi}^{\mathcal{B}} : \rangle}{\int d\phi \langle \hat{n}_{\circ\phi}^{\mathcal{A}} \rangle \int d\phi \langle \hat{n}_{\bullet\phi}^{\mathcal{B}} \rangle}, \quad (16)$$

where $\hat{n} = \hat{a}^\dagger \hat{a}$ is the number density, and \circ, \bullet denote the momentum states of species \mathcal{A} and \mathcal{B} . Due to the cylindrical symmetry of the system, the correlation can be integrated over all azimuthal angles ϕ .

For a Bell test [2, 3, 13, 22], we aim to measure the Bell correlation E between the momentum of the two species. E is defined as the expectation value of the product of the momentum observables of species

\mathcal{A} and \mathcal{B} : $E(\varphi_{\mathcal{A}}, \varphi_{\mathcal{B}}) = \langle \hat{p}_{\mathcal{A}} \hat{p}_{\mathcal{B}} \rangle$, where $\hat{p}_{\mathcal{X}}$ is a two-mode momentum operator of species \mathcal{X} . These operators have normalised eigenvalues of ± 1 , corresponding to the upwards and downwards momentum states of each species. E can then be calculated from the second-order correlation function $g_{\bullet\bullet}^{(2)}$ as

$$E(\varphi_{\mathcal{A}}, \varphi_{\mathcal{B}}) = g_{\nearrow\nearrow}^{(2)} + g_{\searrow\searrow}^{(2)} - g_{\nearrow\searrow}^{(2)} - g_{\searrow\nearrow}^{(2)} \quad (17)$$

$$= \frac{1 - \cos(\varphi_{\mathcal{A}} + \varphi_{\mathcal{B}})}{2} \cos(\theta_{\mathcal{A}} - \theta_{\mathcal{B}}) \quad (18)$$

$$+ \frac{1 + \cos(\varphi_{\mathcal{A}} + \varphi_{\mathcal{B}})}{2} \cos(\theta_{\mathcal{A}} + \theta_{\mathcal{B}}) \\ = \cos(\theta_{\mathcal{A}} + \theta_{\mathcal{B}}) \text{ for } \varphi_{\mathcal{A}} = \varphi_{\mathcal{B}} = 0 \quad (19)$$

for some particular mixing pulse phase settings $\varphi_{\mathcal{A}}$ and $\varphi_{\mathcal{B}}$. To test Bell's inequality, we compute the CHSH parameter \mathcal{S} [3, 35] with four different correlators,

$$\mathcal{S} = E(\varphi_{\mathcal{A}}, \varphi_{\mathcal{B}}) - E(\varphi_{\mathcal{A}}, \varphi'_{\mathcal{B}}) \\ + E(\varphi'_{\mathcal{A}}, \varphi_{\mathcal{B}}) + E(\varphi'_{\mathcal{A}}, \varphi'_{\mathcal{B}}) \quad (20)$$

with each term representing experiments with those specific phase settings. For instance, choosing phases

$$\varphi_{\mathcal{A}} + \varphi_{\mathcal{B}} = \frac{\pi}{4}, \quad \varphi_{\mathcal{A}} + \varphi'_{\mathcal{B}} = \frac{3\pi}{4}, \\ \varphi'_{\mathcal{A}} + \varphi_{\mathcal{B}} = \frac{7\pi}{4}, \quad \varphi'_{\mathcal{A}} + \varphi'_{\mathcal{B}} = \frac{9\pi}{4}, \quad (21)$$

each term in (20) evaluates to $+1/\sqrt{2}$, and $\mathcal{S} = 2\sqrt{2}$, exceeding the local hidden variable theory limit of 2 [3].

3 Simulations

The Split-Step Operator Method. We developed a numerical simulation to model the full experimental sequence, including the Bragg pulses, collisions, and beam-splitter operations. This employs the split-step operator method [36] to solve the time-dependent Schrödinger equation for the two-particle wavefunction of ${}^3\text{He}^*$ and ${}^4\text{He}^*$. The method alternates between applying the kinetic and potential energy operators in small timesteps, allowing efficient and accurate evolution of the wavefunction in time. Chosen for its ability to explicitly compute the entangled state of the two species, this approach is also versatile and can be adapted to other studies involving entanglement in continuous variable systems.

The two-particle wavefunction is discretised on a $2D \otimes 2D$ grid to balance computational efficiency while retaining the scattering halo geometry. The wavefunction is expressed as

$$|\psi(\mathbf{r}, t)\rangle = |\psi(x_3, z_3, x_4, z_4, t)\rangle \quad (22)$$

where x_3, z_3 and x_4, z_4 denote the spatial coordinates of the ${}^3\text{He}^*$ and ${}^4\text{He}^*$ atoms respectively.

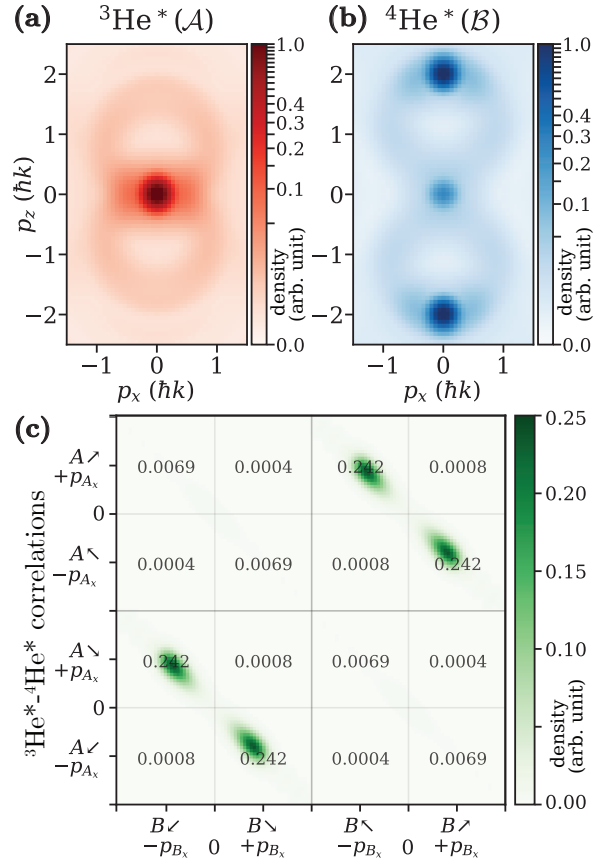


Fig. 2: Numerical simulations of the momentum density distribution of (a) ${}^3\text{He}^*(\mathcal{A})$ and (b) ${}^4\text{He}^*(\mathcal{B})$ immediately after the initial Bragg diffraction and collision show the scattering halos generated from s -wave collisions between atoms of both species. (c) The back-to-back correlations present in the dual-species double halo, calculated by slicing the $2D \otimes 2D$ total momentum wavefunction to $1D \times 1D$, i.e., $|\langle p_z^{\mathcal{A}}, p_z^{\mathcal{B}} | \Phi(p_x^{\mathcal{A}}, p_x^{\mathcal{B}}, p_x^{\mathcal{B}}, p_x^{\mathcal{A}}) \rangle|^2$. By integrating around the selected momentum states, we can calculate each joint detection probability between different momentum states of interest, shown in the overlaid text. These probabilities are used to calculate the Bell correlation (see Eqn. (17)) of this initial state to be $E = 0.94$.

The time evolution of the wavefunction is governed by

$$|\psi(\mathbf{r}, t + dt)\rangle = e^{-\frac{i}{\hbar}(\hat{H}_p + \hat{H}_r)dt} |\psi(\mathbf{r}, t)\rangle \quad (23)$$

where the full Hamiltonian can be split into momentum and position dependences $\hat{H} = \hat{H}_p + \hat{H}_r$. Here $\hat{H}_p = \frac{p^2}{2m}$ represents the kinetic term and \hat{H}_r includes the s -wave scattering and Bragg pulse potentials. Using the split-step operator method, also known as the Zassenhaus or reverse Campbell-Hausdorff expansion [36, 37, 38], the evolution over a time step dt is approximated as

$$|\psi(\mathbf{r}, t + dt)\rangle = e^{-\frac{i}{\hbar}\hat{H}_r \frac{dt}{2}} e^{-\frac{i}{\hbar}\hat{H}_p dt} e^{-\frac{i}{\hbar}\hat{H}_r \frac{dt}{2}} |\psi(\mathbf{r}, t)\rangle \\ + \mathcal{O}(dt^3). \quad (24)$$

For our case, we selected a time step of $0.1\mu\text{s}$ and grid size of 121 points per dimension, providing a spatial resolution of $0.5\mu\text{m}$ and momentum resolution of $0.066\hbar k$, where $k = |\mathbf{k}_1 - \mathbf{k}_2|$ is the wavevector of the Bragg beams. This configuration is a balance between accuracy, with $\mathcal{O}(dt^3)$ error, and computational feasibility, requiring ~ 10 hours runtime on a standard desktop computer to simulate the full experimental duration of $\sim 1.2\text{ms}$, with a memory footprint of $\sim 4\text{GB}$ per wavefunction array.

Simulation of the full experiment. Building on the simulation method described above, we model the full experiment sequence under realistic experimental conditions. The parameters include the laser pulse durations ($50\mu\text{s}$ and $66\mu\text{s}$ for $^3\text{He}^*$ and $^4\text{He}^*$ respectively), intensities ($\sim 0.1\text{mW}/\text{mm}^2$), as well as the atomic scattering properties ($a_{34} = 29\text{nm}$) [28, 33, 39].

Following the scheme described earlier (see Fig. 1), we initialise overlapping degenerate gases of $^3\text{He}^*$ and $^4\text{He}^*$ atoms in the groundstate of the harmonic trapping potential. To simulate the subsequent mirror and beam-splitter, we apply an effective Bragg pulse potential given by $\hat{V}_B = V_B(t) \cos(2\mathbf{k} \cdot \mathbf{x} - \delta t - \varphi)$, where $V_B(t)$ is the pulse envelope, \mathbf{k} is the wavevector, δ is the detuning, and φ is the phase [22].

In Fig. 2.(a) and (b), we show the momentum density distribution of $^3\text{He}^*$ and $^4\text{He}^*$, respectively, immediately after the initial Bragg diffraction and collision, highlighting the resultant s -wave scattering halos. By analysing slices of the wavefunction, we confirm that strong correlations are present in the initial state, as shown by the correlation amplitude plot in Fig. 2.(c).

Observation of Bell correlations. We then add mirror and mixing pulses to simulate the full Bell test sequence with varying mixing pulse transfer fraction θ_A and θ_B to produce the full correlation plot shown in Fig. 3. The correlation function $E(\theta_A, \theta_B)$ closely follows the quantum mechanical prediction of $\cos(\theta_A + \theta_B)$ from Eqn. (19). This shows that our proposed experimental configuration can maintain sufficient phase coherence to perform a Bell test. Specifically, the halo width and the coherence length and time are adequate to preserve the necessary interference effects.

The experimental implementation will use a microchannel plate and delay line detector positioned in the far field to detect individual atoms with high spatial and temporal resolution [40]. The dual-species interferometer spans $\sim 100\mu\text{m}$ in length, while atoms will fall approximately 0.85m to reach the detector, allowing for measurement in the far field with single atom 3D resolution [22, 13]. These far-field positions can be mapped to corresponding velocity and momentum states after the interferometer sequence. We can

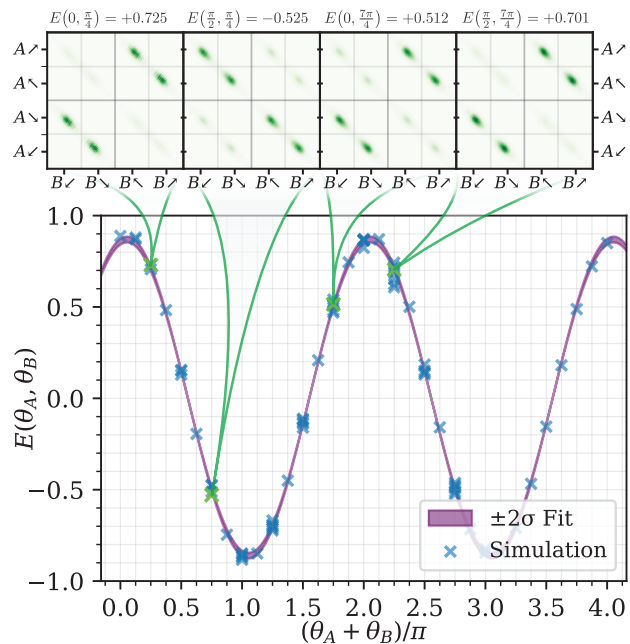


Fig. 3: **(a)** The Bell correlator $E(\theta_A, \theta_B)$ for different transfer proportions of θ_A and θ_B . The simulations show excellent agreement with the quantum prediction of $E = +\cos(\theta_A + \theta_B)$. The four insets show the correlator for the four different phase settings used to calculate the CHSH parameter with a maximal violation. For the four values highlighted, the CHSH value exceeds the classical limit of 2.

apply a magnetic field gradient during free fall to spatially separate the two species [13, 22].

4 Conclusion and Outlook

In conclusion, we have presented a proposal to test a Bell inequality using momentum-entangled pairs of atoms of different masses. The distinct atomic transition frequencies allow independent control of the interferometer phases φ and pulse durations θ for each species, enabling a CHSH-type Bell test that overcomes limitations of previous single-species approaches [22, 16].

Beyond the Bell test, this setup could also test the Weak Equivalence Principle using entangled test masses [41]. By varying the interferometer pulse sequence timings $t_{1,2}^{A,B}$, this setup can measure gravitational phase accumulation during free fall for each species [42, 41]. Furthermore, this setup can be configured to measure Hong-Ou-Mandel (HOM) interference [43], by using two entangled pairs that are scattered in the same direction (Eqn (6) as the initial state). Unlike the photonic case, here both the bosonic ‘‘HOM dip’’ (bunching) and fermionic ‘‘HOM peak’’ (anti-bunching) could be observed in the same experiment.

There is also the potential to advance our understanding of the interaction between gravity and the entangled states of massive objects, such as described

in Eqn. (8) [44]. According to quantum interpretations, the momentum (or position) of these atoms is fundamentally indeterminate until interacted with, and hence the spacetime metric influenced by their mass is also undetermined [45]. Although we are not directly probing quantised gravitational interactions like gravitons [46], a successful Bell test using this massive momentum entangled state would present an experimental observation that any contemporary quantum gravity theory must explain [47, 48]. This lays the groundwork for a new class of experiments that explore the boundaries between quantum mechanics and gravity.

Acknowledgements

The authors would like to thank S.A. Haine for careful reading of the manuscript and J.J. Hope, K.F. Thomas and B.M. Henson for helpful discussions. This work was supported through the Australian Research Council (ARC) Discovery Projects, Grant No. DP190103021, DP240101346 and DP240101441. S.S. Hodgman was supported by the Australian Research Council Future Fellowship Grant No. FT220100670. S. Kannan was supported by an Australian Government Research Training Program scholarship.

References

- [1] A. Einstein, B. Podolsky, and N. Rosen. “Can Quantum-Mechanical Description of Physical Reality Be Considered Complete?”. *Physical Review* **47**, 777–780 (1935).
- [2] J. S. Bell. “On the Einstein Podolsky Rosen paradox”. *Physics Physique Fizika* **1**, 195–200 (1964).
- [3] John F. Clauser, Michael A. Horne, Abner Shimony, and Richard A. Holt. “Proposed Experiment to Test Local Hidden-Variable Theories”. *Physical Review Letters* **23**, 880–884 (1969).
- [4] Alain Aspect, Philippe Grangier, and Gérard Roger. “Experimental Tests of Realistic Local Theories via Bell’s Theorem”. *Physical Review Letters* **47**, 460–463 (1981).
- [5] Alain Aspect, Jean Dalibard, and Gérard Roger. “Experimental Test of Bell’s Inequalities Using Time-Varying Analyzers”. *Physical Review Letters* **49**, 1804–1807 (1982).
- [6] Marco Tomasin, Elia Mantoan, Jonathan Jogenfors, Giuseppe Vallone, Jan-Åke Larsson, and Paolo Villoresi. “High-visibility time-bin entanglement for testing chained Bell inequalities”. *Physical Review A* **95**, 032107 (2017).
- [7] Libby Heaney and Janet Anders. “Bell-inequality test for spatial-mode entanglement of a single massive particle”. *Physical Review A* **80**, 032104 (2009).
- [8] Xiao-Xiao Chen, Qing-Yuan Wu, Zhe Meng, Mairikena Aili, Jian Li, Jia-Zhi Yang, and An-Ning Zhang. “Imaging of Single-Photon Orbital-Angular-Momentum Bell States”. *Physical Review Applied* **18**, 054053 (2022).
- [9] J. G. Rarity and P. R. Tapster. “Experimental violation of Bell’s inequality based on phase and momentum”. *Physical Review Letters* **64**, 2495–2498 (1990).
- [10] J. G. Rarity and P. R. Tapster. “Two-color photons and nonlocality in fourth-order interference”. *Physical Review A* **41**, 5139–5146 (1990).
- [11] M. A. Rowe, D. Kielpinski, V. Meyer, C. A. Sackett, W. M. Itano, C. Monroe, and D. J. Wineland. “Experimental violation of a Bell’s inequality with efficient detection”. *Nature* **409**, 791–794 (2001).
- [12] B. Hensen, H. Bernien, A. E. Dréau, A. Reiserer, N. Kalb, M. S. Blok, J. Ruitenberg, R. F. L. Vermeulen, R. N. Schouten, C. Abellán, W. Amaya, V. Pruneri, M. W. Mitchell, M. Markham, D. J. Twitchen, D. Elkouss, S. Wehner, T. H. Taminiau, and R. Hanson. “Loophole-free Bell inequality violation using electron spins separated by 1.3 kilometres”. *Nature* **526**, 682–686 (2015).
- [13] D. K. Shin, B. M. Henson, S. S. Hodgman, T. Wasak, J. Chwedeńczuk, and A. G. Truscott. “Bell correlations between spatially separated pairs of atoms”. *Nature Communications* **10**, 4447 (2019).
- [14] Roman Schmied, Jean-Daniel Bancal, Baptiste Allard, Matteo Fadel, Valerio Scarani, Philipp Treutlein, and Nicolas Sangouard. “Bell correlations in a Bose-Einstein condensate”. *Science* **352**, 441–444 (2016).
- [15] Luca Pezzè, Augusto Smerzi, Markus K. Oberthaler, Roman Schmied, and Philipp Treutlein. “Quantum metrology with nonclassical states of atomic ensembles”. *Reviews of Modern Physics* **90**, 035005 (2018).
- [16] Pierre Dussarrat, Maxime Perrier, Almazbek Imanaliev, Raphael Lopes, Alain Aspect, Marc Cheneau, Denis Boiron, and Christoph I. Westbrook. “Two-Particle Four-Mode Interferometer for Atoms”. *Physical Review Letters* **119**, 173202 (2017).
- [17] Matteo Fadel, Tilman Zibold, Boris Décamps, and Philipp Treutlein. “Spatial entanglement patterns and Einstein-Podolsky-Rosen steering in Bose-Einstein condensates”. *Science* **360**, 409–413 (2018).
- [18] Karsten Lange, Jan Peise, Bernd Lücke, Ilka Kruse, Giuseppe Vitagliano, Iagoba Apellaniz, Matthias Kleinmann, Géza Tóth, and Carsten

- Klempt. “Entanglement between two spatially separated atomic modes”. *Science* **360**, 416–418 (2018).
- [19] Jiří Tomkovič, Michael Schreiber, Joachim Welte, Martin Kiffner, Jörg Schmiedmayer, and Markus K. Oberthaler. “Single spontaneous photon as a coherent beamsplitter for an atomic matter-wave”. *Nature Physics* **7**, 379–382 (2011).
- [20] L. Slodička, G. Hétet, N. Röck, P. Schindler, M. Hennrich, and R. Blatt. “Atom-Atom Entanglement by Single-Photon Detection”. *Physical Review Letters* **110**, 083603 (2013).
- [21] F. Anders, A. Idel, P. Feldmann, D. Bondarenko, S. Loriani, K. Lange, J. Peise, M. Gersemann, B. Meyer-Hoppe, S. Abend, N. Gaaloul, C. Schubert, D. Schlippert, L. Santos, E. Rasel, and C. Klempt. “Momentum Entanglement for Atom Interferometry”. *Physical Review Letters* **127**, 140402 (2021).
- [22] Kieran F. Thomas, Bryce M. Henson, Yu Wang, Robert J. Lewis-Swan, Karen V. Kheruntsyan, Sean S. Hodgman, and Andrew G. Truscott. “A matter-wave Rarity-Tapster interferometer to demonstrate non-locality”. *The European Physical Journal D* **76**, 244 (2022).
- [23] R. J. Lewis-Swan and K. V. Kheruntsyan. “Proposal for a motional-state Bell inequality test with ultracold atoms”. *Physical Review A* **91**, 052114 (2015).
- [24] Kieran F. Thomas, Zhuoxian Ou, Bryce M. Henson, Angela A. Baiju, Sean S. Hodgman, and Andrew G. Truscott. “Production of a highly degenerate fermi gas of metastable ^3He atoms”. *Physical Review A* **107**, 033313 (2023).
- [25] David M. Giltner, Roger W. McGowan, and Siu Au Lee. “Theoretical and experimental study of the Bragg scattering of atoms from a standing light wave”. *Physical Review A* **52**, 3966–3972 (1995).
- [26] A. Perrin, H. Chang, V. Krachmalnicoff, M. Schellekens, D. Boiron, A. Aspect, and C. I. Westbrook. “Observation of Atom Pairs in Spontaneous Four-Wave Mixing of Two Colliding Bose-Einstein Condensates”. *Physical Review Letters* **99**, 150405 (2007).
- [27] S. S. Hodgman, R. I. Khakimov, R. J. Lewis-Swan, A. G. Truscott, and K. V. Kheruntsyan. “Solving the Quantum Many-Body Problem via Correlations Measured with a Momentum Microscope”. *Physical Review Letters* **118**, 240402 (2017).
- [28] S. Kannan, Y. S. Athreya, A. H. Abbas, X. T. Yan, S. S. Hodgman, and A. G. Truscott. “Measurement of the s -wave scattering length between metastable helium isotopes”. *Physical Review A* **110** (2024).
- [29] Andrei B. Klimov. “A Group-Theoretical Approach to Quantum Optics: Models of Atom-Field Interactions”. *John Wiley & Sons, Incorporated*. Weinheim (2009). 1st ed edition.
- [30] Samuel L. Braunstein and Peter Van Loock. “Quantum information with continuous variables”. *Reviews of Modern Physics* **77**, 513–577 (2005).
- [31] Wu RuGway, S. S. Hodgman, R. G. Dall, M. T. Johnsson, and A. G. Truscott. “Correlations in Amplified Four-Wave Mixing of Matter Waves”. *Physical Review Letters* **107**, 075301 (2011).
- [32] F. C. Khanna, J. M. C. Malbouisson, A. E. Santana, and E. S. Santos. “Maximum entanglement in squeezed boson and fermion states”. *Physical Review A* **76**, 022109 (2007).
- [33] J. M. McNamara, T. Jeltens, A. S. Tychkov, W. Hogervorst, and W. Vassen. “Degenerate Bose-Fermi Mixture of Metastable Atoms”. *Physical Review Letters* **97**, 080404 (2006).
- [34] Kieran F. Thomas, Shijie Li, A. H. Abbas, Andrew G. Truscott, and Sean S. Hodgman. “ n -body antibunching in a degenerate fermi gas of $^3\text{He}^*$ atoms”. *Physical Review Research* **6**, L022003 (2024).
- [35] A. Aspect. “Proposed experiment to test separable hidden-variable theories”. *Physics Letters A* **54**, 117–118 (1975).
- [36] James Schloss. “Massively parallel split-step fourier techniques for simulating quantum systems on graphics processing units”. PhD Thesis (2019).
- [37] Wilhelm Magnus. “On the exponential solution of differential equations for a linear operator”. *Communications on Pure and Applied Mathematics* **7**, 649–673 (1954). [arXiv:https://onlinelibrary.wiley.com/doi/pdf/10.1002/cpa.31](https://onlinelibrary.wiley.com/doi/pdf/10.1002/cpa.31)
- [38] Fernando Casas, Ander Murua, and Mladen Nadinic. “Efficient computation of the zassenhaus formula”. *Computer Physics Communications* **183**, 2386–2391 (2012).
- [39] T. M. F. Hirsch, D. G. Cocks, and S. S. Hodgman. “Close-coupled model of feshbach resonances in ultracold $^3\text{He}^*$ and $^4\text{He}^*$ atomic collisions”. *Physical Review A* **104**, 033317 (2021).
- [40] A. G. Manning, S. S. Hodgman, R. G. Dall, M. T. Johnsson, and A. G. Truscott. “The Hanbury Brown-Twiss effect in a pulsed atom laser”. *Optics Express* **18**, 18712 (2010).
- [41] Remi Geiger and Michael Trupke. “Proposal for a Quantum Test of the Weak Equivalence Principle with Entangled Atomic Species”. *Physical Review Letters* **120**, 043602 (2018).

- [42] Achim Peters, Keng Yeow Chung, and Steven Chu. “Measurement of gravitational acceleration by dropping atoms”. *Nature* **400**, 849–852 (1999).
- [43] C. K. Hong, Z. Y. Ou, and L. Mandel. “Measurement of subpicosecond time intervals between two photons by interference”. *Physical Review Letters* **59**, 2044–2046 (1987).
- [44] Daniel Carney, Philip C E Stamp, and Jacob M Taylor. “Tabletop experiments for quantum gravity: A user’s manual”. *Classical and Quantum Gravity* **36**, 034001 (2019).
- [45] M Carlesso, A Bassi, M Paternostro, and H Ulbricht. “Testing the gravitational field generated by a quantum superposition”. *New Journal of Physics* **21**, 093052 (2019).
- [46] C. Marletto and V. Vedral. “Gravitationally Induced Entanglement between Two Massive Particles is Sufficient Evidence of Quantum Effects in Gravity”. *Physical Review Letters* **119**, 240402 (2017).
- [47] Houri Ziaeeepour. “Comparing Quantum Gravity Models: String Theory, Loop Quantum Gravity, and Entanglement Gravity versus $SU(\infty)$ -QGR”. *Symmetry* **14**, 58 (2022).
- [48] S Carlip. “Is quantum gravity necessary?”. *Classical and Quantum Gravity* **25**, 154010 (2008).